UNIVERSITY OF LEEDS

Article:
Yazdi, R, Ghasemi, HM, Wang, C et al. (1 more author) (2017) Bio-corrosion behaviour of oxygen diffusion layer on Ti-6Al-4V during tribocorrosion. Corrosion Science, 128. pp. 23-32. ISSN 0010-938X

https://doi.org/10.1016/j.corsci.2017.08.031

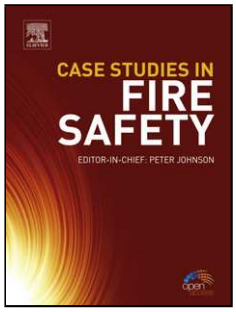

Title: Bio-corrosion behaviour of oxygen diffusion layer on Ti-6Al-4V during tribocorrosion

Authors: R. Yazdi, H.M. Ghasemi, C. Wang, A. Neville

PII: S0010-938X(17)31151-4
DOI: http://dx.doi.org/10.1016/j.corsci.2017.08.031
Reference: CS 7184

To appear in:

Received date: 28-6-2017
Revised date: 22-8-2017
Accepted date: 23-8-2017

Please cite this article as: R.Yazdi, H.M.Ghasemi, C.Wang, A.Neville, Bio-corrosion behaviour of oxygen diffusion layer on Ti-6Al-4V during tribocorrosion, Corrosion Sciencehttp://dx.doi.org/10.1016/j.corsci.2017.08.031

Bio-corrosion behaviour of oxygen diffusion layer on Ti-6Al-4V during tribocorrosion

R. Yazdi[a], H.M. Ghasemi[a]*, C. Wang[b] and A. Neville[b]

a School of Metallurgy and Materials Engineering, College of Engineering, University of Tehran, Tehran, Iran

b Institute of Functional Surfaces, School of Mechanical Engineering, University of Leeds, Leeds, LS2 9JT, UK

*Corresponding author. Tel.: +98 2161114095, E-mail address: hghasemi@ut.ac.ir (H.M. Ghasemi).

Highlights

- **Nano-hardness increased in ODLs formed at a temperature of 850°C for 3 and 6 hours.**
- **A bilayer film on Ti-6Al-4V and ODLs led to a very low i_{corr} in a stagnant PBS.**
- **E_{corr} and i_{corr} in Ti-6Al-4V were affected by work hardening during tribocorrosion.**
- **Under tribocorrosion, lowest i_{corr} was obtained in 3hr-ODL.**

Abstract

Oxygen diffusion layers (ODL) on Ti-6Al-4V were produced by thermal oxidation at a temperature of 850 °C for three and six hours. ODL formation resulted in a β-Ti to α-Ti transformation, causing an increase in hardness. Polarization and EIS studies in stagnant and tribocorrosion conditions were performed under normal loads of 3-30 N in a phosphate buffered saline solution. In a stagnant condition, a passive bilayer film was formed on samples, which led to a low i_{corr}. During tribocorrosion, the formation of a protective tribofilm resulted in a higher E_{corr} and a lower i_{corr} in ODLs compared with Ti-6Al-4V.

Keywords: A. Titanium; A. Ceramic; B. Polarization ; B. EIS; C. Hardening; C. Effects of strain

1. Introduction

Titanium-based alloys have various applications in the medical industries especially as implants. This is due to their low density, excellent corrosion resistance and their good biocompatibility [1–3]. In medical applications, the poor tribological properties of titanium are a drawback, where the passive film can be destroyed by mechanical loading [4]. This releases different detrimental ions into the human body [5]. Wear may affect corrosion as follows: a) passive film removal by tribological action [6], b) work hardening and higher surface energy production [7], (c) roughness increase which results in a greater surface area exposed to the corrosive medium and an increase in pit stability [8]. To study the change in corrosion behaviour during tribocorrosion, there are five different electrochemical techniques: (1) OCP measurement, (2,3) potentiodynamic/potentiostatic tests, (4) electrochemical impedance spectroscopy (EIS) and (5) electrochemical noise determination (ECN) [9]. Among them, the potentiodynamic polarization test is the most effective way to quantify the corrosion rate, which may be enhanced by wear.

A wide variety of investigations have been performed to improve wear resistance of titanium and its alloys. As an easy and atmospheric friendly technique, the thermal oxidation process could be used to improve the tribological behaviour of titanium alloys [10]. Titanium has a high affinity to oxygen to bond and to share their valance electrons in order to decrease its energy and become more stable. At a high temperature, the kinetics of oxidation generally increase and the formation of oxide layer may largely improve nano-hardness, nano-scratch and the fretting wear resistance of titanium alloys [11]. The oxidation parameters need to be appropriately selected in order to form a sound oxide layer strongly adhered to substrate [12]. The oxidation of Ti-6Al-4V has

promoted the tribocorrosion resistance, 25 times greater than the untreated sample in a wear test conducted in a 0.9% NaCl solution. The titanium oxide layer also causes low coefficient of friction during tribocorrosion than untreated titanium by changing the wear mechanism [13]. However, titanium oxide can bear extremely low applied forces in a tribological situation due to its fragile nature [14,15].

During the oxidation, oxygen can dissolve in titanium up to 34 at%, according to the Ti-O phase diagram [16]. Therefore, high temperature processing of titanium in atmospheric conditions results in an oxygen diffusion layer (ODL) covered by titanium oxide [17,18]. In Ti-O solid solution, oxygen atoms are placed in the octahedral positions and diffused by the passway of hexahedral and nonbasal crowdion positions [19]. The oxygen diffusion layer is considered to have better wear resistance than titanium oxide at high loads and larger sliding distances [18]. A Boost Diffusion Oxidation (BDO) technique has been developed by Dong et al. [20] and improved by Zhang et al. [21], in which they hardened titanium surface by two steps (I) thermal oxidation and (II) heat treatment in high vacuum. They found that ODL could effectively improve the dry wear resistance of titanium up to four times [22,23]. The tribological behaviour of the oxygen hardened layer on Ti-6Al-4V in ZDDP lubricated conditions was assessed in another investigation [24]. The results showed that a tribofilm could be formed on the surface which avoided the substrate having direct contact with its counterpart.

To best of our knowledge, tribo-electrochemical assessment of oxygen diffusion layer on Ti-6Al-4V has not been presented in the literature, only a few studies have been reported on the tribological behaviour of ODL formed on Ti–6Al–4V alloy [15,23]. In this study, the oxygen diffusion layer was produced by thermal oxidation at the temperature of 850 °C for three and six hours and their corrosion behaviour in stagnant and tribocorrosion conditions were investigated in a phosphate buffered saline solution.

2. Experimental Procedure

Ti-6Al-4V samples as disks were provided with 32 mm in diameter. The chemical composition of the Ti-6Al-4V material was obtained by Optical Emission Spectroscopy (OES) and is listed in Table 1. The samples were polished to a roughness average (Ra) of 0.14±0.03 μm. The specimens were placed in an atmospheric furnace at a temperature of 850 °C, just below α to β phase transformation temperature of the material, for three and six hours. The specimens were then air quenched at room temperature to easily remove the loosely adhered oxide layer from the substrate to reveal the oxygen diffusion layers (i.e., 3hr-ODL and 6hr-ODL). Figure 1 shows the fragmentation of oxide layer during quenching step, which was detached from the substrate. Some small scale oxide fragments remained on the surface, which were further removed by a light polishing.

The microstructure of the cross sections of ODL samples was studied using Scanning Electron Microscopy (SEM), Energy Dispersive Spectroscopy (EDS). Changes in hardness of the ODL samples were also measured by a nano-hardness tester, at an applied load of 10 mN and loading/unloading rate of 0.2 mN/s. In addition, the elastic modulus (E) of the ODL samples were also measured from the load vs. penetration depth curves.

The corrosion tests of treated (i.e., ODL) and Ti-6Al-4V specimens were conducted in a Phosphate Buffered Saline (PBS) solution in a stagnant condition and during tribocorrosion at room temperature. PBS was prepared in accordance with ASTM F2129 [25], with a composition of 8.0 g/L NaCl, 0.2 g/L KCl, 1.15 g/L Na_2HPO_4 and 0.2 g/L KH_2PO_4 in distillated water. The tribocorrosion tests were performed against alumina ball with a diameter of 5 mm and a hardness of 1550 Hv using a Ball-on-Disk tribometer under normal loads of 3, 7.5, 15, 30 N at a sliding

speed of 0.1 m/s. Figure 2 schematically represents the tribocorrosion set-up; installed on the tribometer. The rig and the polymeric samples holders were designed for accurate measurement of electrochemical signals during tribocorrosion. The signals were obtained by an Autolab potentionstat/galvanostat with the help of NOVA software, version 1.9. The corrosion tests in the stagnant and tribocorrosion conditions were conducted in a three-electrode cell; the specimens as a working electrode, Ag/AgCl and platinum as the reference and counter electrode, respectively. The distance between the reference, the counting and the working electrodes (i.e., sample) was about 2 cm during both stagnant and tribocorrosion tests.

The specimens were immersed in a stagnant PBS for one hour to stabilize the Open Circuit Potential (OCP), and the polarization measurements were then obtained with a scan rate of 0.16 mV/s. The polarization tests during tribocorrosion were obtained after five minutes of sliding, with a scan rate of 1 mV/s from -700 mV to about +2000 mV, relative to OCP.

Electrochemical Impedance Spectroscopy (EIS) of the specimens was performed in a frequency range of 10 kHz to 0.01 Hz with amplitudes of 5 and 30 mV versus open-circuit potential in the stagnant and tribocorrosion conditions, respectively. The EIS spectra were recorded with data logging of 7 electrochemical signals per frequency decade. Before EIS, the OCP of the specimens was stabilized with the same procedure as used for the polarization tests in the stagnant and tribocorrosion conditions. The nano-hardness tests, EDS analyses, the tribocorrosion and electrochemical experiments were repeated for at least three times and the mean values and standard deviations were calculated.

To obtain the corrosion current density (i_{corr}), the corrosion current (i.e., I_{corr}) was divided by the area of the wear track. The apparent area of wear tracks was calculated using the width of wear track measured by a stylus profilometer multiplied by its average perimeter. The area outside of

the wear track was assumed to be a reference; due to insignificant values of the passive current (i.e., outside of wear track), compared with that for the wear area. The area of the wear tracks was also used to normalize the impedance data (i.e., Z, Z' and Z") obtained from the EIS experiments.

3. Results and Discussion

3.1. Microstructure of ODLs

Figure 3 shows SEM micrographs of the cross sections of 3hr-ODL and 6hr-ODL following the thermal oxygen treatment at a temperature of 850 °C for three and six hours, respectively. The decreasing trend of the amount of dissolved oxygen with distance from surface of the samples in Fig. 3 is illustrated in the EDS analysis of Fig. 4. There were three distinct zones shown in Fig. 3 depending on the amount of oxygen diffusion. Zones I and II were affected by oxygen diffusion forming ODLs, whereas Zone III was not affected by oxygen (i.e., (α+β)-Ti). Zone III was essentially the same as Ti-6Al-4V with a (α+β) microstructure containing mostly α-Ti grains with an untransformed β-Ti precipitated in α-Ti grain boundaries [1,26,27]. Oxygen is an alpha stabilizing element with a solubility limit of 34 at% and 0.8-3.4 at% in α-Ti and β-Ti, respectively [16]. Therefore, with a high amount of oxygen near surface (Fig. 4) during heat treatment, β-Ti could be promptly saturated by oxygen and the transformation of oxygen-saturated β-Ti to an unsaturated α-Ti also called alpha casing [28] subsequently occurred in zone I. Figure 3 also shows that the thermal oxidation treatment caused a growth of alpha phase in a deeper area, i.e., zone II, as a result of β to α transformation. The amount of this transformation was less (i.e., more β-Ti) due to lower oxygen diffusion in zone II. However, as the diffusion time increased from 3 to 6 hours, zone I extended deeper followed by zone II. The formation of alpha-case

(zone I) and oxygen-rich layer in (α+β)-Ti (zone II) by thermal oxidation were also reported by Satko [28].

EDS point analysis of the dissolved oxygen at various depths of the cross sections in both ODL samples is shown in Fig. 4. There were two oxygen gradient regions; i) maximum oxygen content at the near surface region was sharply dropped to the depth corresponding to the stabilized alpha region (zone I), and ii) a lower oxygen variation was observed in the deeper regions (zone II). This was due to the presence of beta phase with a higher oxygen diffusion coefficient [26] in zone II which led to a higher oxygen diffusion rate and the lower oxygen gradient.

3.2. Nano-Mechanical Properties of the ODLs

The nano-indentation tests were performed on Ti6Al4V and the ODL samples. The nano-hardness values were calculated from the variation of indentation load as a function of penetration depth for the samples [29]. The nano-hardness profiles of the cross section of ODL samples are shown in Fig. 5. Maximum hardness of 10.0±0.28 GPa (1030±30 Hv) and 19.0±3.5 GPa (1950±350 Hv) was measured for 3hr-ODL and 6hr-ODL at the near surface regions, respectively, as compared with a value of 5.4±0.34 GPa (550±35 Hv) obtained for Ti-6Al-4V before oxygen heat treatment. Oxygen as a solute element produces a solid solution with titanium. Oxygen with a small atomic radius could be placed at interstitial sites (octahedral sites) of hcp structure of titanium leading to a large distortion of crystal structure [30]. The distorted structure under stress, i.e., in measurement of the indentation hardness, could hinder plastic flow [19] and, therefore, increase the hardness. Comparing Figs. 4 and 5 reveals that the change in hardness was directly related to oxygen content where a higher oxygen content resulted in a higher hardness. The extracted data at any depth from

the surface could approximate the following empirical equation showing the change of the nano-hardness with the dissolved oxygen in Ti-6Al-4V alloy.

$$H\ (GPa) = 0.71 \times O\ (at\%) + k \qquad \text{Equation (1)}$$

Where H is the nano-hardness, O is oxygen content in atomic percent and k is the time dependent parameter, which was 5.5 and 8.5 for 3hr-ODL and 6hr-ODL, respectively.

3.3. Corrosion in stagnant condition

The potentiodynamic polarization tests were conducted in PBS in a stagnant condition and the resultant curves are presented in Fig. 6. All three samples exhibited low corrosion current density of about 90-143 nA/cm^2 and corrosion potential of about -150 mV vs. Ag/AgCl, indicating that the thermal processing had no adverse effect in kinetic and tendency of corrosion in PBS. This could mean that the corrosion behaviour and osseointegration of the ODLs are similar to Ti-6Al-4V in the human body in static applications.

The very limited values of corrosion current densities, i_{corr}, (less than 150 nA/cm^2) for the samples also revealed the presence of a passive film on the samples [31]. This was also confirmed by the existence of a passive area in the anodic branches. However, the polarization curves illustrated the passive areas with different features in the three samples. In Ti-6Al-4V, the passive current density value (i_p) was found to be constant in the anodic potential range between +300 mV and +1480 mV vs. Ag/AgCl. The ODLs showed about 60% lower values of passive current density than Ti-6Al-4V, which might be due to the formation of a more protective layer [32].

Figure 6 shows that as the heat treatment time was increased from three to six hours, there was a more pronounced change in the slope of the passive area of the anodic branch at the potentials

lower than +1500 mV vs. Ag/AgCl. This was due to the presence of a higher amount of metastable titanium oxides (Ti_XO_Y) on the surface of 6hr-ODL, which were oxidized to form TiO_2 at different potential steps [33]. Beside producing titanium (IV) ion, titanium could be presented with lower valances according to reaction (1) [34]. Therefore, titanium oxides other than TiO_2 could be formed during the heat treatment just beneath TiO_2 layer according to reaction (2). These oxides could remain on the ODL surfaces after the air quenching and removal of TiO_2 layer due to a strong adhesion between the oxides and the substrates [34]. During polarization, when the required driving force was obtained by the higher anodic potentials, these oxides could react with water to form TiO_2 in accordance with reaction (3). This resulted in a slight increase in anodic current densities over the applied potential range as happened more pronouncedly in 6hr-ODL.

$$Ti \rightarrow Ti^{n+} + n\bar{e} \ (n \leq 4) \qquad \text{Reaction (1)}$$

$$X\ Ti + Y/2\ O_2 \rightarrow Ti_XO_Y \qquad \text{Reaction (2)}$$

$$A\ Ti_XO_Y + B\ H_2O \rightarrow C\ TiO_2 + 2B\ H^+ + 2B\ \bar{e} \qquad \text{Reaction (3)}$$

At potentials higher than +1500 mV vs. Ag/AgCl, there was an increase in anodic current densities for the three samples. It is suggested that the increase in current densities at the higher potentials is not the indication of transpassive phenomena (i.e., the destruction of the passive film by oxygen evolution) in titanium based alloys [35,36]. This was due to the formation of a new passive layer made of phosphorous containing titanium complex [31] in the stagnant PBS solution.

Figure 7 exhibits the Bode spectra from EIS data for the untreated (Ti-6Al-4V) and diffusion treated (ODL) samples in a stagnant PBS solution. The Bode modulus spectra represent almost the same resistance in impedance modulus (i.e., |Z|) over the applied frequency range for the samples. This could indicate a similar corrosion behaviour for all three samples, as previously indicated by the polarization curves in Fig. 6. In addition, the peak angle in the Bode phase pattern

for Ti-6Al-4V was close to -90°, indicating a good capacitive behavior [37] of the passive film in PBS. The peaks of about -70° phase angle for the two ODLs were resulted from the same capacitive behaviour of passive films. The Bode phase spectra for Ti-6Al-4V and the ODLs also show broad peaks over a large range of frequency. This could be attributed to cumulative capacitive effect of more than one time constant which was resulted from the formation of a passive film [35].

The passive film formed on titanium in aqueous solution is often mentioned as a TiO_2 [38], however, other investigations have further mentioned the formation of a two-layer film on Ti-6Al-4V in PBS corrosive medium [39]. This concept was used to fit and simulate the EIS data for the samples with a relevant equivalent circuit. The simulated equivalent circuit for Ti-6Al-4V and the ODL samples was appropriately fitted in the Bode spectra, as shown in Fig. 7. The electrochemical parameters obtained from the simulations results are listed in Table 2. The chi-square (χ^2) of less than 0.01 also indicated a good accuracy of the simulated and actual EIS data [40]. A constant phase element (CPE) is defined as non-ideal capacitor due to the distribution of surface reactivity, the heterogeneous surfaces and roughness, the electrode porosity and geometry. They all may have an influence on distribution of electrochemical current and potential [41]. The n having a value less than one specifies the deviation of CPE from an ideal capacitor, i.e., a lower value of n indicates a more deviated CPE from an ideal capacitor [42]. As listed in Table 2, the values of n_1 and n_2 for Ti-6Al-4V were obtained to be closer to one than those for the ODLs. This was due to a lower average surface roughness (Ra) of about 0.14±0.03 μm for Ti-6Al-4V, as compared with R_a of 0.47±0.05 μm for both ODLs, revealing a more ideal capacitive behaviour for Ti-6Al-4V. A greater deviation from ideal capacitor (i.e., with a phase angle of -90 degree) for the ODLs was also confirmed by a lower peak angle in the Bode phase spectra.

The relatively low resistance (R_{out}) of outer layer and significant higher resistance (R_{in}) of inner layer of the passive film for the samples in Table 2 could indicate a very defective or porous outer layer coupled by a relatively dense inner layer [35,39]. This also confirmed the existence of two time constants in the circuit model, which resulted from the titanium oxide bilayer. This was in good agreement with the previous results as reported by other investigators [31,37]. The ODLs with higher R_{in} values represented a better protective film properties and a higher corrosion resistance. The higher capacitance of the passive film (CPE2) on the ODL samples could be attributed to their higher surface roughness, as compared with Ti-6Al-4V sample [43]. On the other hand, the capacitance of passive film (i.e., CPE2) is reciprocally related to the thickness [44], therefore, a lower value of CPE2 for Ti-6Al-4V, in Table 2, could also indicate the formation of a thicker passive layer compared with the ODL samples. It is suggested that although the thinner layers might be formed in the ODL samples, the conductivity was lowered, as indicated by the higher R_{in} values in Table 2. This also suggested the formation of a more compact passive layer on the ODL samples compared with Ti-6Al-4V.

3.4. Tribocorrosion behaviour

Figure 8 presents the polarization curves of Ti-6Al-4V and the ODLs during tribocorrosion under different normal loads. The figure shows a passive zone in the anodic branch for all specimens. However, the higher current densities of about two to three orders of magnitude over the applied potentials compared with the stagnant condition (Fig. 6) indicated a higher electrochemical reaction rates accelerated by wear processing. Figure 8 shows a large fluctuation in anodic current density in the passive zone for Ti-6Al-4V, which was lowered as the normal load was increased. This could be related to a sequential depassivation/repassivation in Ti-6Al-4V [45] during sliding. It seems that there was a higher reactivity of Ti-6Al-4V under higher normal loads resulting in a

more protective tribolayer, which consequently reduced the fluctuations of the current densities in the anodic branch of the polarization curves.

Figure 8 also shows that the current fluctuations in the anodic branch of polarization curves in the ODL samples were comparably lower than Ti-6Al-4V. The ODL surfaces with higher hardness and strength could better support the tribolayer formed during sliding. This could result in a lower ploughing and deformation leading to a more durable tribolayer, which limited depassivation/repassivation variation and, therefore, smaller current fluctuations in the ODL samples. Figs. 8c and d show a higher slope in the passive region of the ODLs' polarization curves under normal loads of 15 and 30 N compared with normal loads of 3 and 7.5 N. This was attributed to a better removal of unstable oxides such as TiO and Ti_3O_4 [34] by wear under the higher normal loads. Therefore, a lower amount of these oxides were oxidized to TiO_2 over the passive potential range. As the anodic potential increased, the lower amount of oxidation limited the increase in the anodic current densities in the passive area and consequently resulted in a higher passive slope.

The corrosion potentials (E_{corr}) and corrosion current densities (i_{corr}) for both the stagnant and tribocorrosion conditions were determined from the polarization curves by Tafel extrapolation method and are shown in Figs. 9 and 10, respectively. Figure 9 shows a lower (i.e., a higher negative) corrosion potential during wear under various normal loads, indicating a higher tendency to corrosion as compared with that in the stagnant condition. The local removal of the film formed during tribocorrosion by the mechanical loads during wear could bring the partially bare surface into contact with the solution, leading to a higher susceptibility to corrosion attack. Figure 9 also shows that as the normal load was increased, the corrosion potential was also decreased probably due to a higher deformation obtained under a higher normal load leading to a higher tendency to corrosion.

Table 3 shows the ratio of the worn to unworn surface area, which was the ratio of the surface affected by wear to the rest of the sample disk surface under various loads. The ratio was increased by increasing the normal loads, causing a decrease in corrosion potential as shown in Fig. 9. The highest decrease in corrosion potential under a specific normal load (Fig. 9) occurred in Ti-6Al-4V due to a larger wear surface area (i.e., higher ratio of the worn to unworn surface area) obtained among the samples. The ratio was lower in ODL samples probably due to their higher hardness and limited plastic deformation, which also resulted in a higher corrosion potential in the ODLs. Table 3 shows that only the test under a normal load of 30 N for 6hr-ODL shows a smaller wear surface area (i.e., a lower worn to unworn ratio) compared with the two other samples, however, its corrosion potential was not the highest (Fig. 9). This will be discussed later.

Figure 10 shows that there were about two to three orders of magnitude increase in the corrosion current density during the tribocorrosion compared with the stagnant condition under various normal loads. Furthermore, the figure shows that, for example, as the load was increased from 3 to 30 N, the corrosion current density of Ti-6Al-4V decreased by about 30%. Table 4 shows the difference between the hardness measured about 500 nm beneath the wear track and the hardness at the same depth from the unworn surface (Fig. 5). For example, under a normal load of 30 N, the wear depth of about 28 µm was measured by surface profilometer for 3hr-ODL. Therefore, the difference in hardness of about 600 (5.9 GPa) just beneath the wear track and a hardness of about 520 Hv (5.1 GPa) 28 µm away from the unworn surface from Fig. 5, resulted in a value of 80 Hv (0.8 GPa) shown in Table 4. The table shows that the difference in hardness increased as the normal load increased. The increase of hardness during wear might be due to effects of work-hardening and change in physical properties of wear surface by the formation of a tribolayer [46]. During wear, the plastic deformation of Ti-6Al-4V was led to an increase in work hardening and hardness (Table 4). In the ODLs, however, the oxygen atoms presented in interstitial site of

titanium limited the change in hardness by limiting the plastic deformation and work hardening during wear [47]. A higher difference in hardness and, therefore, a higher work hardening occurred in Ti-6Al-4V as the normal load increased. The higher change in hardness of Ti-6Al-4V wear surface could enable the surface to better support the tribolayer formed by the corrosion and wear phenomena [7]. The formation of a durable tribolayer could result in a reduction in corrosion current density (i_{corr}) of Ti-6Al-4V under a higher normal load shown in Fig. 10.

Figure 10 shows that i_{corr} in 3hr-ODL unexpectedly decreased as the normal load increased from 15 to 30 N during tribocorrosion. In 6hr-ODL, on the other hand, there was an increasing trend in corrosion current densities with the increase of the normal load and the highest i_{corr} was resulted under a normal load of 30 N. SEM images of wear tracks of the samples under a normal load of 30 N show three different surface features as shown in Fig. 11. EDS analysis of the wear surface of the samples in Fig. 11 is listed in Table 5. The table shows higher amount of oxygen than the unworn surfaces (Fig. 4) indicating the formation of tribological oxide layers on the samples under a normal load of 30 N. An excessive plastic deformations was taken place on the Ti-6Al-4V wear track (Fig. 11a), which caused a remarkable increase of about 380 Hv in the hardness respect to undeformed surface according to Table 4. The tribological action in 3hr-ODL formed a smooth wear surface, on which a protective tribolayer was formed and resulted in a lower corrosion current density. Figures 11c and d show a different wear mechanism for 6hr-ODL under a normal load of 30 N. The figures reveal fractures on the wear surface, which could lead to a surface with a higher roughness and a larger effective surface area exposed to the corrosive medium during wear. However, the apparent surface area of wear track, which was smaller than the actual effective surface area was considered in the calculations of the corrosion current density. This could result in a higher corrosion current density in 6hr-ODL under a normal load of 30 N than 3hr-ODL shown in Fig. 10. Furthermore, the higher actual effective surface area also resulted in a more negative

potential [48] shown in Fig. 9. The nano-hardness measurement of 6hr-ODL shows higher hardness (Fig. 5) and much higher elastic modulus of about 195 GPa than that for 3hr-ODL (i.e., about 165 GPa). This led to a lower E/H value for 6hr-ODL, resulting in a more brittle sliding wear behaviour [49] of 6hr-ODL shown in Figs. 11c and d. The results from Table 4 show that there was a softening or a reduction in hardness following the sliding by about 380 Hv just beneath 6hr-ODL wear surface under a normal load of 30 N as compared with the hardness of the unworn area. It seems that the hardness obtained just beneath the wear surface was measured within the fractured layers caused by sliding, therefore indicating a low hardness at that region.

EDS analysis of the wear surface of the samples under a normal load of 30 N listed in Table 5 shows that the elements of oxygen and phosphorous were presented on the wear surfaces. This could be due to tribo-chemical reactions occurred during tribocorrosion, which probably resulted in a tribolayer in all three samples. There was a high oxygen content of about 70 at% on the wear surface of 3hr-ODL (Fig. 11b) and region 1 in Fig. 11d corresponding to the wear surface of 6hr-ODL. Although the diffused oxygen in the ODLs could be responsible for the high oxygen content of the ODL wear surfaces, however, this value was much higher than the maximum oxygen of the unworn ODLs (less than 20 at%) shown in Fig. 5. The higher oxygen could be due to the presence of a tribolayer rich in oxide on the wear surface of 3hr-ODL and 6hr-ODL. On the other hand, EDS analysis of point 2 on the fractured area in Fig. 11d shows a lower oxygen and no phosphorous contents as compared with point 1. The removal of the tribolayer at the fractured region could make the surface more susceptible to corrosion and could lead to a higher corrosion current density under the normal load of 30 N (Fig. 10). In addition, the lowest corrosion current densities was obtained in 3hr-ODL under various normal loads in Fig. 10. This was probably due to the limited plastic deformation (Table 4) and the formation of a protective tribolayer during tribocorrosion as occurred under a normal load of 30 N. In 3hr-ODL, there was an increase in i_{corr}

by about two times under normal loads of 7.5 and 15 N, as compared with a normal load of 3 N. It could indicate that the tribolayer was not as protective under the higher loads, resulting in an increase in corrosion current density.

The EIS data of the ODLs under various normal loads were plotted and Nyquist spectra are illustrated in Fig. 12. It should be reported that an accurate study of electrochemical behaviour of Ti-6Al-4V by EIS was not possible during tribocorrosion. This was due to high depassivation/repassivation of the alloy shown in Fig. 8, which resulted in a high fluctuation (i.e., of more than 30 mV) in the corrosion potential. The semi-cycles in Nyquist diagrams were depressed over the entire frequency range under various normal loads, which indicated a deviation from ideal capacitor [50]. This was mainly related to the roughening of surface during tribocorrosion [51]. The semi-circle of 3hr-ODL under a normal load of 3 N in Fig. 12a shows the highest diameter, indicating the highest corrosion resistance. A larger semi-circle under a normal load of 30 N was resulted from the higher corrosion resistance of 3hr-ODL compared with those under normal load of 7.5 and 15 N. This was also confirmed by the lower i_{corr} under a normal load of 30 N (Fig. 10) due to the formation of a protective tribolayer (Fig. 11b and Table 5) on the wear surface under this load.

Figure 12b shows that the corrosion resistance of 6hr-ODL decreased as the normal load increased and there was a lowest corrosion resistance under a normal load of 30 N. The fracture on the wear surface (Figs. 11c and d) led to a higher corrosion current density (Fig. 10) and, therefore, a lowest corrosion resistance.

4. Conclusions

(1) The microstructure of the ODLs showed two diffusion regions, alpha enrichment in the near surface and alpha with a remained beta titanium in deeper area; which increased the surface hardness of Ti-6Al-4V from 5.4 GPa to 10.1 and 19.1 GPa in 3hr-ODL and 6hr-ODL, respectively.

(2) There was no change in the corrosion current density by the thermal oxidation treatment in the stagnant PBS solution as indicated in polarization curves and confirmed by the EIS data.

(3) The polarization and EIS data obtained during tribocorrosion revealed higher corrosion current densities as well as more negative corrosion potentials as compared with stagnant condition.

(4) Under various normal loads in Ti-6Al-4V, corrosion was influenced by work hardening during tribocorrosion. On the other hand, the lowest corrosion current densities were obtained in 3hr-ODL among the samples due to a limited plastic deformation and the formation of a protective tribolayer.

(5) Under a normal load of 30 N, different wear mechanisms resulted in large differences between corrosion current densities for the samples. The durable tribolayer on the wear surface resulted in a lowest corrosion current density in 3hr-ODL. The highest corrosion current density was obtained in 6hr-ODL due to the presence of surface fracture and partial removal of the tribolayer by wear.

(6) During tribocorrosion, it was demonstrated that the decrease in corrosion potentials was directly related to the worn-to-unworn surface ratio. Due to a limited plastic deformation, ODLs had a lower ratio and, therefore, showed a higher corrosion potential as compared with Ti-6Al-4V.

5. References

[1] M. Long, H.J. Rack, Titanium alloys in total joint replacement—a materials science perspective., Biomaterials. 19 (1998) 1621–1639. doi:10.1016/S0142-9612(97)00146-4.

[2] M. Geetha, a. K. Singh, R. Asokamani, a. K. Gogia, Ti based biomaterials, the ultimate choice for orthopaedic implants - A review, Prog. Mater. Sci. 54 (2009) 397–425. doi:10.1016/j.pmatsci.2008.06.004.

[3] M. Abdel-Hady Gepreel, M. Niinomi, Biocompatibility of Ti-alloys for long-term implantation, J. Mech. Behav. Biomed. Mater. 20 (2013) 407–415. doi:10.1016/j.jmbbm.2012.11.014.

[4] R. Yazdi, S.F. Kashani-Bozorg, Microstructure and wear of in-situ Ti/(TiN + TiB) hybrid composite layers produced using liquid phase process, Mater. Chem. Phys. 152 (2015). doi:10.1016/j.matchemphys.2014.12.026.

[5] G. Pezzotti, K. Yamamoto, Artificial hip joints: The biomaterials challenge, J. Mech. Behav. Biomed. Mater. 31 (2014) 3–20. doi:10.1016/j.jmbbm.2013.06.001.

[6] V. Totolin, V. Pejaković, T. Csanyi, O. Hekele, M. Huber, M. Rodríguez Ripoll, Surface engineering of Ti6Al4V surfaces for enhanced tribocorrosion performance in artificial seawater, Mater. Des. 104 (2016) 10–18. doi:10.1016/j.matdes.2016.04.080.

[7] J. Chen, F.Y. Yan, B.B. Chen, J.Z. Wang, Assessing the tribocorrosion performance of Ti-6Al-4V, 316 stainless steel and Monel K500 alloys in artificial seawater, Mater. Corros. 64 (2013) 394–401. doi:10.1002/maco.201106249.

[8] E. Arslan, Y. Totik, E. Demirci, A. Alsaran, Influence of surface roughness on corrosion and tribological behavior of CP-Ti after thermal oxidation treatment, J. Mater. Eng. Perform. 19 (2010) 428–433. doi:10.1007/s11665-009-9504-9.

[9] S. Mischler, Triboelectrochemical techniques and interpretation methods in tribocorrosion: A comparative evaluation, Tribol. Int. 41 (2008) 573–583. doi:10.1016/j.triboint.2007.11.003.

[10] Y. Luo, W. Chen, M. Tian, S. Teng, Thermal oxidation of Ti6Al4V alloy and its biotribological properties under serum lubrication, Tribol. Int. 89 (2015) 67–71. doi:10.1016/j.triboint.2014.12.022.

[11] S. Wang, Z. Liao, Y. Liu, W. Liu, Influence of thermal oxidation duration on the microstructure and fretting wear behavior of Ti6Al4V alloy, Mater. Chem. Phys. 159 (2015) 139–151. doi:10.1016/j.matchemphys.2015.03.063.

[12] M. Jamesh, S. Kumar, T.S.N. Sankara Narayanan, Effect of Thermal Oxidation on Corrosion Resistance of Commercially Pure Titanium in Acid Medium, J. Mater. Eng. Perform. 21 (2011) 902–907. doi:10.1007/s11665-011-9970-8.

[13] R. Bailey, Y. Sun, Corrosion and Tribocorrosion Performance of Thermally Oxidized Commercially Pure Titanium in a 0.9% NaCl Solution, J. Mater. Eng. Perform. 24 (2015) 1669–1678. doi:10.1007/s11665-015-1441-1.

[14] S. Kumar, T.S.N.S. Narayanan, S.G. Sundara, S.K. Seshadri, Fretting corrosion behaviour of thermally oxidized CP-Ti in Ringer's solution, Corros. Sci. 52 (2010) 711–721. doi:10.1016/j.corsci.2009.10.029.

[15] H. Güleryüz, H. Çimenoğlu, Effect of thermal oxidation on corrosion and corrosion-wear behaviour of a Ti-6Al-4V alloy, Biomaterials. 25 (2004) 3325–3333. doi:10.1016/j.biomaterials.2003.10.009.

[16] F.H. Froes, ed., Principles of Alloying Titanium, in: Titan. Phys. Metall. Process. Appl., First Edit, ASM International, Ohio, 2015: pp. 51–74.

[17] P. Stratton, M. Graf, Wear of diffusion hardened Ti-6Al-4V sliding against tool steel, Wear. 268 (2010) 612–616. doi:10.1016/j.wear.2009.10.009.

[18] R. Bailey, Y. Sun, Unlubricated sliding friction and wear characteristics of thermally oxidized commercially pure titanium, Wear. 308 (2013) 61–70. doi:10.1016/j.wear.2013.09.020.

[19] H.H. Wu, D.R. Trinkle, Direct diffusion through interpenetrating networks: Oxygen in titanium, Phys. Rev. Lett. 107 (2011) 1–4. doi:10.1103/PhysRevLett.107.045504.

[20] H. Dong, X.Y. Li, Oxygen boost diffusion for the deep-case hardening of titanium alloys, Mater. Sci. Eng. A. 280 (2000) 303–310. doi:10.1016/S0921-5093(99)00697-8.

[21] Z.X. Zhang, H. Dong, T. Bell, B. Xu, The effect of treatment condition on boost diffusion of thermally oxidised titanium alloy, J. Alloys Compd. 431 (2007) 93–99. doi:10.1016/j.jallcom.2006.05.045.

[22] H. Dong, T. Bell, Enhanced wear resistance of titanium surfaces by a new thermal oxidation treatment, Wear. 238 (2000) 131–137. doi:10.1016/S0043-1648(99)00359-2.

[23] F. Borgioli, E. Galvanetto, F. Iozzelli, G. Pradelli, Improvement of wear resistance of Ti-6Al-4V alloy by means of thermal oxidation, Mater. Lett. 59 (2005) 2159–2162. doi:10.1016/j.matlet.2005.02.054.

[24] J. Qu, P.J. Blau, J.Y. Howe, H.M. Meyer, Oxygen diffusion enables anti-wear boundary film formation on titanium surfaces in zinc-dialkyl-dithiophosphate (ZDDP)-containing lubricants, Scr. Mater. 60 (2009) 886–889. doi:10.1016/j.scriptamat.2009.02.009.

[25] ASTM F2129-15, Standard Test Method for Conducting Cyclic Potentiodynamic Polarization Measurements to Determine the Corrosion Susceptibility of Small Implant, 2015.

[26] R.M. Pilliar, Metallic biomaterials, Biomed. Mater. (2009) 41–81. doi:10.1007/978-0-387-84872-3_2.

[27] H. Krawiec, V. Vignal, J. Loch, P. Erazmus-vignal, Influence of plastic deformation on the microstructure and corrosion behaviour of Ti–10Mo –4Zr and Ti–6Al – 4V alloys in the Ringer's solution at 37 ° C, Corros. Sci. 96 (2015) 160–170. doi:10.1016/j.corsci.2015.04.006.

[28] D.P. Satko, J.B. Shaffer, J.S. Tiley, S.L. Semiatin, A.L. Pilchak, S.R. Kalidindi, et al., Effect of microstructure on oxygen rich layer evolution and its impact on fatigue life during high-temperature application of α/β titanium, Acta Mater. 107 (2016) 377–389.

doi:10.1016/j.actamat.2016.01.058.

[29] A.C. Fischer-Cripps, Nanoindentation, Third Edit, Springer Science & Business Media, London, 2011. doi:10.1007/978-1-4419-9872-9.

[30] J. Kratochvil, H. Conrad, Strengthening of Alpha Titanium by Interstitial Solutes, Scr. Mater. 4 (1970) 815–824. doi:10.1016/0036-9748(70)90067-0.

[31] S.L. De Assis, S. Wolynec, I. Costa, Corrosion characterization of titanium alloys by electrochemical techniques, Electrochim. Acta. 51 (2006) 1815–1819. doi:10.1016/j.electacta.2005.02.121.

[32] A. Balyanov, J. Kutnyakova, N.A. Amirkhanova, V. V Stolyarov, R.Z. Valiev, Corrosion resistance of ultra fine-grained Ti, 51 (2004) 225–229. doi:10.1016/j.scriptamat.2004.04.011.

[33] I. Ramires, A.C. Guastaldi, Study of Ti-6Al-4V biomaterial using electrochemistry and XPS techniques, Quim. Nova. 25 (2002) 10–14. doi:10.1590/S0100-40422002000100003.

[34] I.M. Pohrelyuk, V.M. Fedirko, O. V. Tkachuk, R. V. Proskurnyak, Corrosion resistance of Ti-6Al-4V alloy with nitride coatings in Ringer's solution, Corros. Sci. 66 (2013) 392–398. doi:10.1016/j.corsci.2012.10.005.

[35] V.A. Alves, R.Q. Reis, I.C.B. Santos, D.G. Souza, T. de F. Gonçalves, M.A. Pereira-da-Silva, et al., In situ impedance spectroscopy study of the electrochemical corrosion of Ti and Ti-6Al-4V in simulated body fluid at 25 °C and 37 °C, Corros. Sci. 51 (2009) 2473–2482. doi:10.1016/j.corsci.2009.06.035.

[36] I. Hacisalihoglu, A. Samancioglu, F. Yildiz, G. Purcek, A. Alsaran, Tribocorrosion properties of different type titanium alloys in simulated body fluid, Wear. 332–333 (2014) 1–8. doi:10.1016/j.wear.2014.12.017.

[37] T.M. Manhabosco, S.M. Tamborim, C.B. dos Santos, I.L. Müller, Tribological, electrochemical and tribo-electrochemical characterization of bare and nitrided Ti6Al4V in simulated body fluid solution, Corros. Sci. 53 (2011) 1786–1793. doi:10.1016/j.corsci.2011.01.057.

[38] N. Khayatan, H.M. Ghasemi, M. Abedini, Synergistic erosion-corrosion behavior of commercially pure titanium at various impingement angles, Wear. 380–81 (2017) 154–162. doi:doi.org/10.1016/j.wear.2017.03.016.

[39] J. Pan, D. Thierry, C. Leygraf, Electrochemical impedance spectroscopy study of the passive oxide film on titanium for implant application, Electrochim. Acta. 41 (1996) 1143–1153. doi:10.1016/0013-4686(95)00465-3.

[40] D. Mareci, R. Chelariu, G. Ciurescu, D. Sutiman, D.M. Gordin, T. Gloriant, Corrosion behaviour of some titanium dental alloys synthesized by cold crucible levitation melting, J. Optoelectron. Adavnced Mater. 12 (2010) 1590–1596.

[41] J.-B. Jorcin, M.E. Orazem, N. Pébère, B. Tribollet, CPE analysis by local electrochemical impedance spectroscopy, Electrochim. Acta. 51 (2006) 1473–1479. doi:10.1016/j.electacta.2005.02.128.

[42] M.F. Montemor, M.G.S. Ferreira, Electrochemical study of modified bis-

[triethoxysilylpropyl] tetrasulfide silane films applied on the AZ31 Mg alloy, Electrochim. Acta. 52 (2007) 7486–7495. doi:10.1016/j.electacta.2006.12.086.

[43] B. Yoo, K.R. Shin, D.Y. Hwang, D.H. Lee, D.H. Shin, Effect of surface roughness on leakage current and corrosion resistance of oxide layer on AZ91 Mg alloy prepared by plasma electrolytic oxidation, Appl. Surf. Sci. 256 (2010) 6667–6672. doi:10.1016/j.apsusc.2010.04.067.

[44] J.E.G. González, J.C. Mirza-Rosca, Study of the corrosion behavior of titanium and some of its alloys for biomedical and dental implant applications, J. Electroanal. Chem. 471 (1999) 109–115. doi:10.1016/S0022-0728(99)00260-0.

[45] J. Komotori, N. Hisamori, Y. Ohmori, The corrosion/wear mechanisms of Ti-6Al-4V alloy for different scratching rates, Wear. 263 (2007) 412–418. doi:10.1016/j.wear.2006.11.025.

[46] N. Espallargas, S. Mischler, Tribocorrosion behaviour of overlay welded Ni-Cr 625 alloy in sulphuric and nitric acids: Electrochemical and chemical effects, Tribol. Int. 43 (2010) 1209–1217. doi:10.1016/j.triboint.2009.12.009.

[47] S. Zabler, Interstitial Oxygen diffusion hardening - A practical route for the surface protection of titanium, Mater. Charact. 62 (2011) 1205–1213. doi:10.1016/j.matchar.2011.10.012.

[48] F. Contu, B. Elsener, H. Böhni, A study of the potentials achieved during mechanical abrasion and the repassivation rate of titanium and Ti6Al4V in inorganic buffer solutions and bovine serum, Electrochim. Acta. 50 (2004) 33–41. doi:10.1016/j.electacta.2004.07.024.

[49] I. Hutchings, Tribology-Friction and Wear of Engineering Materials, First Edit, Butterworth-Heinemann, London, 1992.

[50] O. Belahssen, A. Chala, H. Ben Temam, S. Benramache, Corrosion and wear resistance of 32CrMoV13 steel nitrided by plasma, RSC Adv. 4 (2014) 52951–52958. doi:10.1039/C4RA08326A.

[51] M. Abedini, H.M. Ghasemi, Corrosion behavior of Al-brass alloy during erosion – corrosion process : Effects of jet velocity and sand concentration, (2016) 513–521. doi:10.1002/maco.201508511.

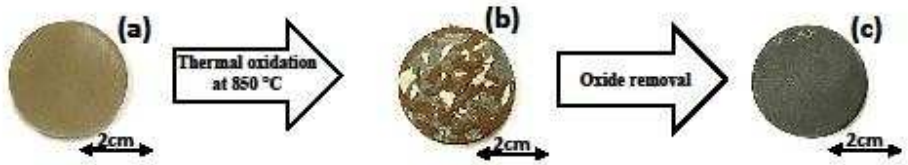

Fig. 1. Typical surface of specimen; (a) before, (b) after thermal processing at 850 °C and (c) after oxide removal showing ODL surface.

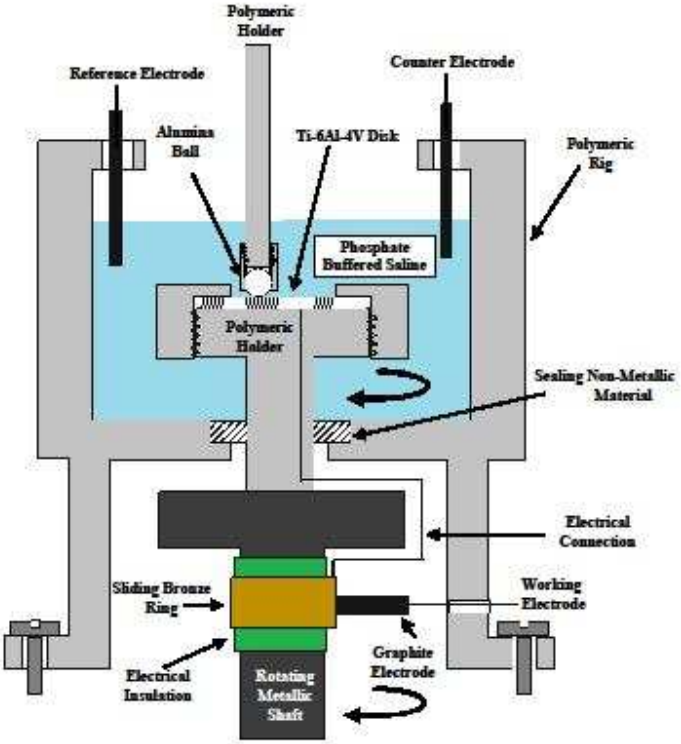

Fig. 2. Schematic illustration of tribocorrosion set-up mounted on Ball-on-Disk tribometer to detect electrochemical signals.

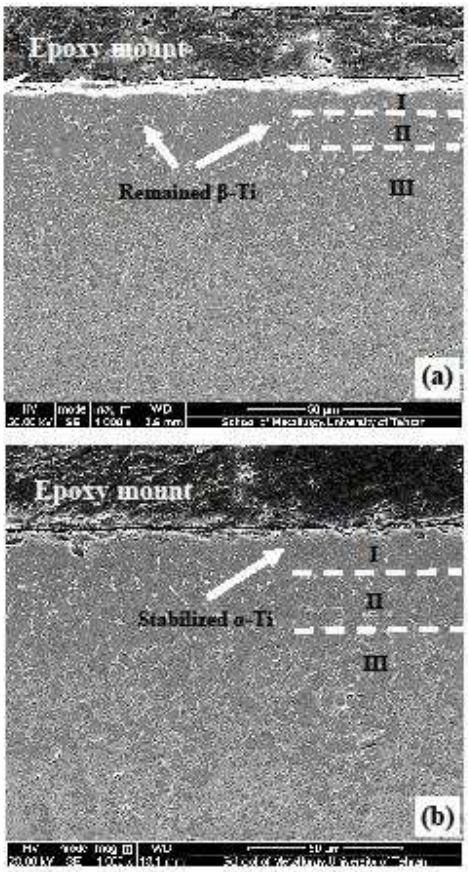

Fig. 3. SEM micrographs of cross section of oxygen diffusion layer (ODL) formed at a temperature of 850 °C for (a) three hours (3hr-ODL) and (b) six hours (6hr-ODL); consisting of three regions: I) stabilized alpha phase at near surface; II) alpha with some amount of remained beta in the area away from the surface and III) highest amount of beta unaffected by oxygen diffusion.

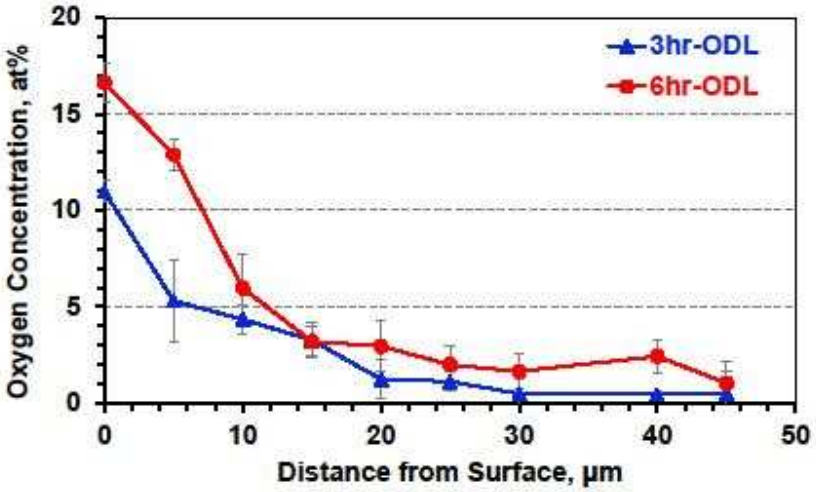

Fig. 4. Variation of Oxygen concentration with depth for 3hr-ODL and 6hr-ODL using EDS analysis.

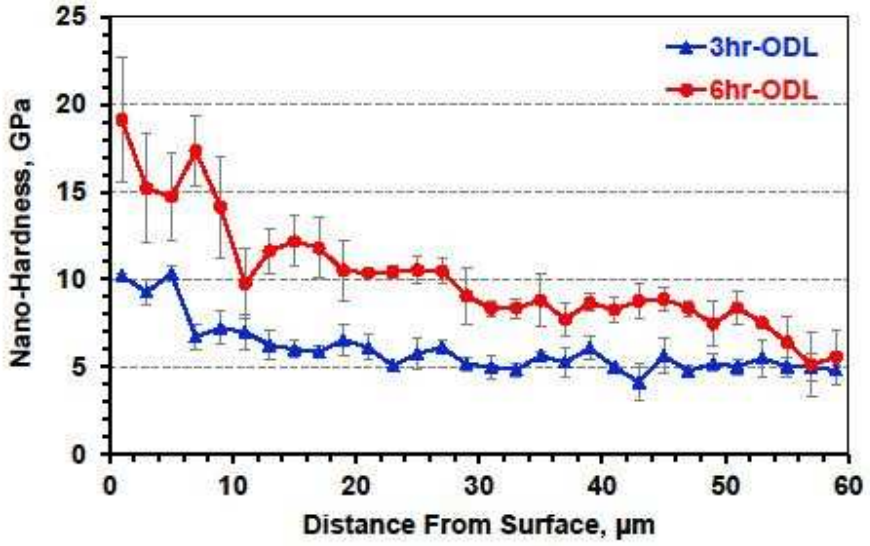

Fig. 5. Nano-hardness profiles of oxygen diffusion layers for 3hr-ODL and 6hr-ODL heat treated at a temperature of 850 °C.

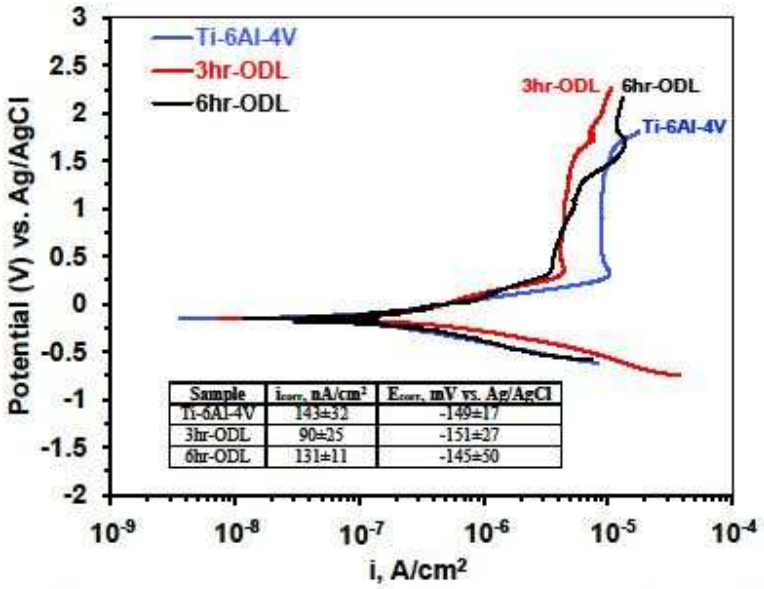

Fig. 6. Potentiodynamic polarization curve of Ti-6Al-4V sample, oxygen diffusion layer formed at 850 °C for three hours (3hr-ODL) and six hours (6hr-ODL) in stagnant PBS solution. The table shown in the figure is the measured values obtained from the polarization curves.

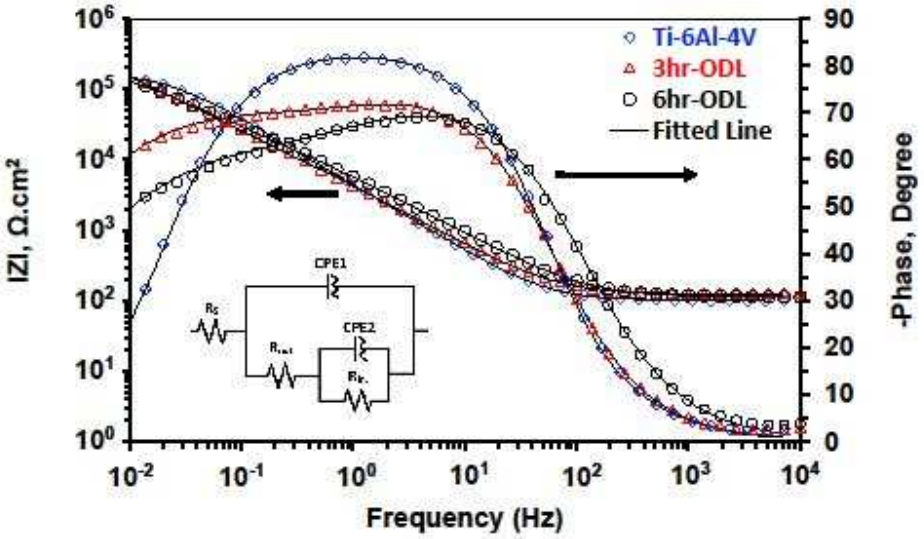

Fig. 7. Bode phase, Bode modulus spectra and simulated patterns according to equivalent circuit for Ti-6Al-4V sample, oxygen diffusion layer formed at 850 °C for three (3hr-ODL) and six hours (6hr-ODL) in stagnant condition. The parameters in the equivalent circuit are: Rs: Resistance of PBS solution; R_{out}: Resistance of outer layer of passive film; R_{in}: Resistance of inner layer of passive film; CPE1: Constant phase element of the outer layer of the passive film and CPE2: Constant phase element related to the inner layer of the passive film.

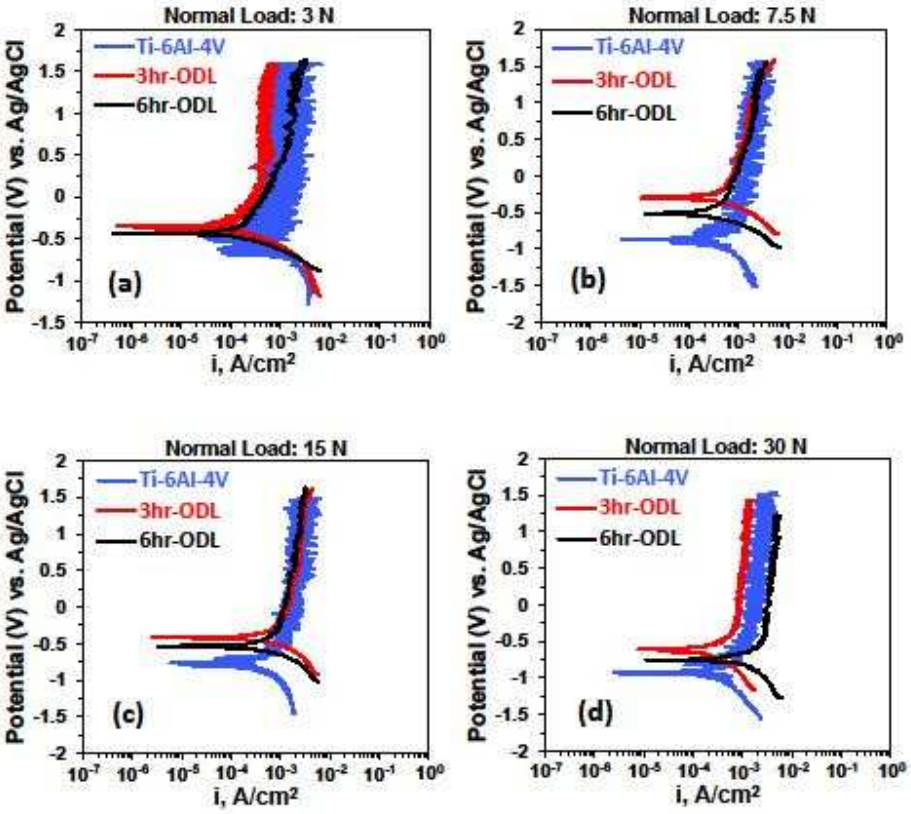

Fig. 8. Potentiodynamic polarization curves of Ti-6Al-4V sample, oxygen diffusion layer formed at 850 °C for three hours (3hr-ODL) and six hours (6hr-ODL) in tribocorrosion conditions under a normal load of (a) 3 N, (b) 7.5 N, (c) 15 N and (d) 30 N.

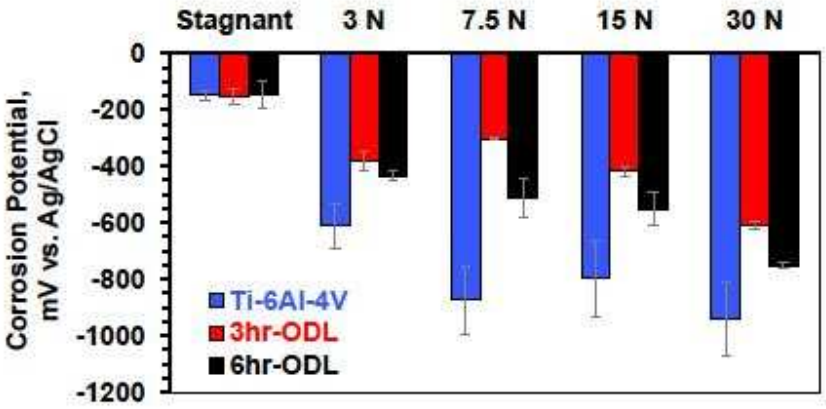

Fig. 9. Corrosion potentials of Ti-6Al-4V, 3hr-ODL and 6hr-ODL in the stagnant and tribocorrosion conditions.

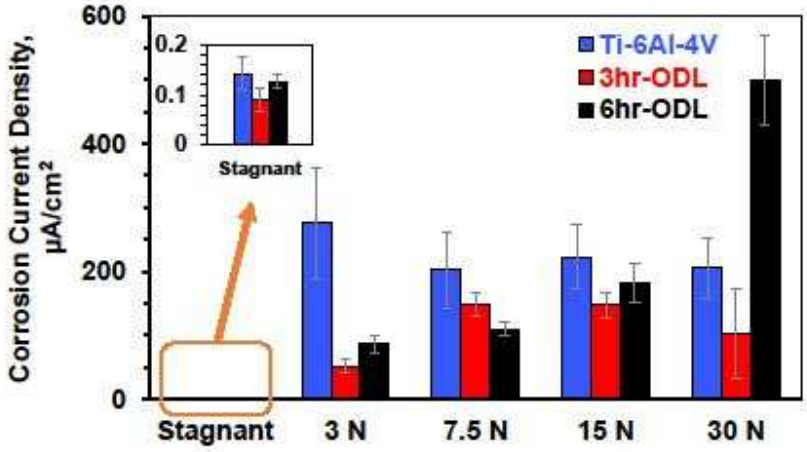

Fig. 10. Corrosion current densities of Ti-6Al-4V, 3hr-ODL and 6hr-ODL in the stagnant and tribocorrosion conditions.

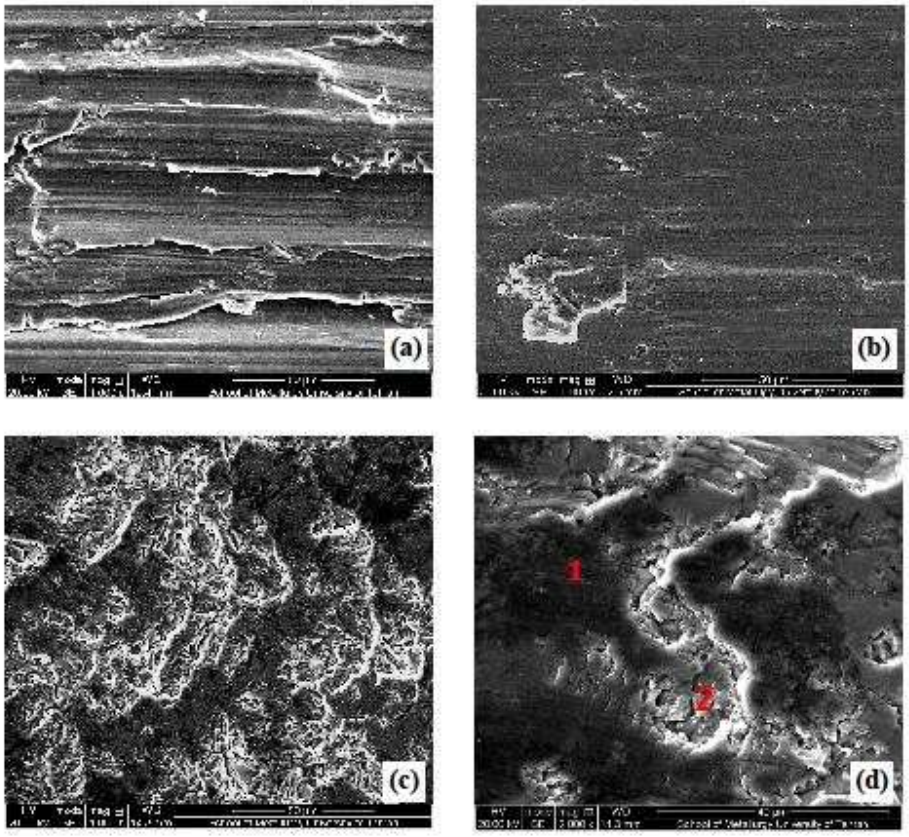

Fig. 11. SEM images of wear tracks (a) Ti-6Al-4V alloy, oxygen diffusion layer formed at the temperature of 850 °C for; (b) three hours, (c) six hours and (d) the same as c at a higher magnification under a normal load of 30 N during tribocorrosion.

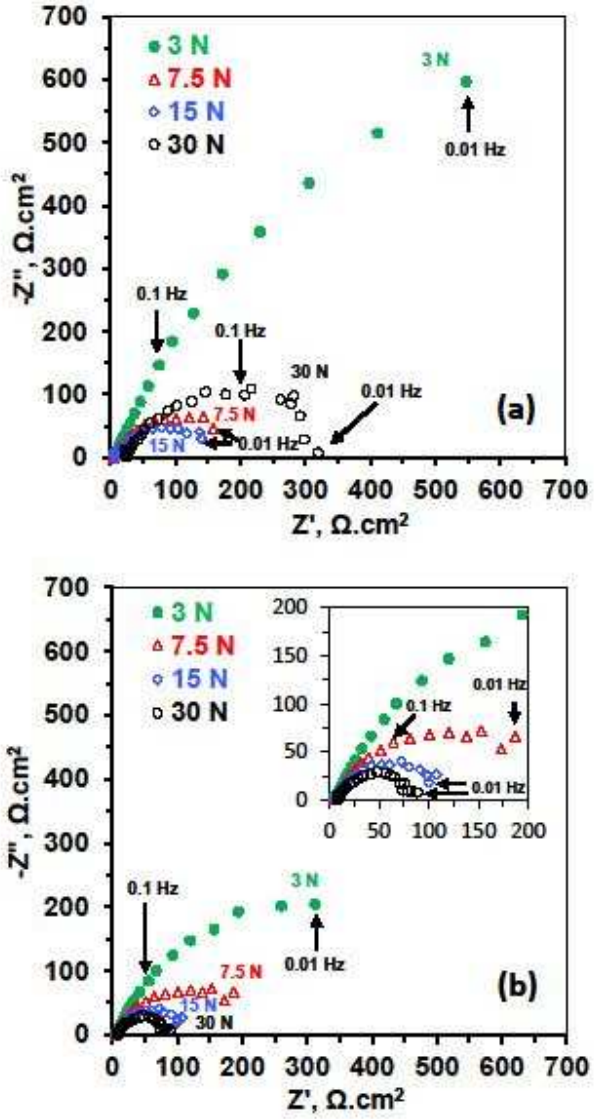

Fig. 12. Nyquist spectra for; (a) 3hr-ODL and (b) 6hr-ODL under various normal loads.

Table 1. Chemical composition of Ti-6Al-4V alloy (wt%).

Ti	Al	V	Fe	Mo	Si	Cu	W	Nb	Ni	Sn	Mn
Base	6.37	4.33	0.03	0.01	0.01	0.01	<0.01	0.008	<0.005	<0.005	<0.004

Table 2. EIS spectra results based on fitted curves on experimental EIS data according to the equivalent circuit in Fig. 7.

Sample	**R_s, $\Omega.cm^2$**	**CPE1, $\mu\Omega^{-1}.cm^{-2}.s^n$**	**n_1**	**R_{out}, $k\Omega.cm^2$**	**CPE2, $\mu\Omega^{-1}.cm^{-2}.s^n$**	**n_2**	**R_{in}, $k\Omega.cm^2$**	**χ^2**
Ti-6Al-4V	99	11.97	0.94	21.6	8.69	0.93	738.9	7.3×10^{-3}
3hr-ODL	123	35.15	0.87	23.2	23.55	0.78	791.9	5.3×10^{-4}
6hr-ODL	112	31.96	0.85	17.5	26.96	0.70	778.5	6.2×10^{-3}

Rs: Resistance of PBS solution; R_{out}: Resistance of outer layer of passive film; R_{in}: Resistance of inner layer of passive film;
CPE1: Constant phase element of the outer layer of the passive film; n_1: The deviation of CPE1 from ideal capacitor (n=1);
CPE2: Constant phase element related to the inner layer of the passive film; n_2: The deviation of CPE2 from ideal capacitor (n=1);
χ^2: The parameter shows the deviation of equivalent circuit data from the experimental results.

Table 3. Ratio of worn-to-unworn surface area in Ti-6Al-4V, 3hr-ODL and 6hr-ODL after tribocorrosion tests.

Normal Load	**Ti-6Al-4V**	**3hr-ODL**	**6hr-ODL**
3 N	0.041±0.002	0.039±0.004	0.036±0.003
7.5 N	0.098±0.005	0.042±0.004	0.047±0.003
15 N	0.150±0.011	0.052±0.004	0.059±0.002
30 N	0.203±0.013	0.117±0.007	0.071±0.007

Table 4. Difference between nano-hardness (Hv)* of the samples at a depth of about 500 nm below the wear surface under various normal loads and the unworn area at the same depth.

Normal Load	Ti-6Al-4V	3hr-ODL	6hr-ODL
3 N	+45±10	Negligible	Negligible
7.5 N	+180±28	Negligible	Negligible
15 N	+190±38	+65±17	+30±15
30 N	+380±36	+80±20	-380±99

*1 Hv = 0.0098 GPa

Table 5. EDS analysis (at%) of wear surfaces in Fig. 11 under a normal load of 30 N; (a) Ti-6Al-4V alloy, (b) 3hr-ODL and (c) 6hr-ODL

Sample	Ti	O	Al	V	P
Ti-6Al-4V	59.2	29.0	10.3	1.1	0.4
3hr-ODL	26.1	68.5	3.6	0.5	1.3
6hr-ODL (point 1 in Fig. 11d)	21.1	66.2	8.0	0.5	4.2
6hr-ODL (point 2 in Fig. 11d)	54.2	38.8	5.8	1.2	0.0